



HAL
open science

Experimental pseudo-equivalent deterministic excitation method extension for low frequency domain applications

Giulia Mazzeo, Giuseppe Petrone, Francesco Franco, Sergio de Rosa,
Mohamed Ichchou, Olivier Bareille

► To cite this version:

Giulia Mazzeo, Giuseppe Petrone, Francesco Franco, Sergio de Rosa, Mohamed Ichchou, et al.. Experimental pseudo-equivalent deterministic excitation method extension for low frequency domain applications. Journal of the Acoustical Society of America, 2023, 154 (6), pp.3507-3520. 10.1121/10.0022375 . hal-04590032

HAL Id: hal-04590032

<https://hal.science/hal-04590032v1>

Submitted on 4 Nov 2024







HAL is a multi-disciplinary open access archive for the deposit and dissemination of scientific research documents, whether they are published or not. The documents may come from teaching and research institutions in France or abroad, or from public or private research centers.

L'archive ouverte pluridisciplinaire **HAL**, est destinée au dépôt et à la diffusion de documents scientifiques de niveau recherche, publiés ou non, émanant des établissements d'enseignement et de recherche français ou étrangers, des laboratoires publics ou privés.



Distributed under a Creative Commons Attribution - NonCommercial 4.0 International License

Experimental pseudo-equivalent deterministic excitation method extension for low frequency domain applications

Giulia Mazzeo,^{1,a)}  Giuseppe Petrone,²  Francesco Franco,²  Sergio De Rosa,²  Mohamed N. Ichchou,¹ 
and Olivier Bareille¹ 

¹Laboratoire de Tribologie et Dynamique des Systèmes, Ecole Centrale de Lyon Ecully 69130, France

²PASTA LAB—Laboratory for Promoting Experiences in Aeronautical Structures and Acoustics, University “Federico II” of Naples, Naples 80125, Italy

ABSTRACT:

In transport engineering applications, flow-induced vibrations is an interesting topic to address since it may negatively affect the operation and the response of the system. Wind tunnel facilities are mandatory to test the structure design efficiency or to analyse new material performances under aerodynamic load. However, these experimental tests can be expensive and take a long time to set up and operate; hence, alternative methods for the reproduction of the structural response to a turbulent boundary layer excitation are required to accelerate and improve the experimental setups and provide more data for uncertainty analysis. In this paper, an alternative approach, the eXperimental Pseudo-Equivalent Deterministic Excitation method (X-PEDE_M), is here extended for applications in the low frequency domain. An investigation about the applicability of the method in the low frequency domain is conducted, together with an analysis of its main properties. The reliability of the method is then tested numerically by considering different conditions: two different panels, two different boundary conditions, and different asymptotic flow velocities are considered.

I. INTRODUCTION

In transport-related industrial fields, such as aviation, marine, railways, and automotive, some of the fundamental problems under study concern air-borne and structure-borne sound emission due to fluid–structure interaction.

Indeed, the flow-induced vibrations might cause several issues, such as structural fatigue, emitted noise at the exterior and interior of a vehicle, and consequently, discomfort of passengers and noise pollution. For these reasons, the prediction of the structural response to wall-pressure fluctuations (WPFs) generated by a turbulent boundary layer (TBL), is one of the main targets of research. The topic presents its difficulties, since the TBL excitation is a random broadband pressure field, represented as a stochastic distribution with a spatial correlation that depends on the convective flow (Bull, 1996). Until today, no *pure* analytical formulations can describe the TBL excitation, but researchers rely on semi-empirical models—represented as the 2-points cross-spectral density (CSD) function (Chase, 1980; Corcos, 1963; Mellen, 1990) or 1-point power spectral density (PSD) function (Goody, 2004)—that depend on empirical data collected for the description of the convective velocity and the decay coefficients. Each model has a different accuracy in the description of the TBL excitation, depending on which frequency range or which asymptotic flow velocity is considered. Hence, when experimental results obtained in a wind tunnel need to be validated, it is often necessary to find first which

model is more suitable to use and then measure the experimental data related to the decay coefficients and convective velocity in order to complete the analytical description of the TBL excitation (Hambric and Lysak, 2019).

From a numerical point of view, the application of these semi-empirical models can be computationally time consuming when exploited in a finite element analysis (FEA) and subjected to limitations of representations in a broadband frequency domain (De Rosa and Franco, 2008).

From an experimental point of view, tests in wind tunnel facilities are still a mandatory step in order to either validate final structural designs or to investigate new material solutions and detect their performances when subjected to an aerodynamic load. They require long and difficult setups for the experiments and a careful choice of the reference model that would better validate the experimental results.

The interest in alternative methods capable to predict the structural response to a TBL excitation rose up with the intention of improving the experimental setups and facilities and doing uncertainty analyses on the data, obtaining a more efficient analysis and more a more performing design process of structures.

One of the first attempts was made by Fahy (1966), who proposed the use of loudspeakers for the WPFs simulation, even though a large number of speakers is required (Maury *et al.*, 2004). Consequently, Aucejo *et al.* (2012) introduced a system to synthetically re-create an array of loudspeakers, considering that a TBL excitation might be approximated to a summation of an infinite number of uncorrelated wall plane waves (UWPWs). This concept was further explored in

^{a)}Email: giulia.mazzeo@ec-lyon.fr

studies by Marchetto *et al.* (2017, 2018), Karimi *et al.* (2020), and Karimi *et al.* (2021). It is essential to understand that the UWPWs method can predict the structural response to TBL excitation, but within a frequency range that begins above the convective coincidence frequency. In this frequency region, TBL can be approximated as a diffuse field, and the spatial correlation is entirely uncorrelated.

Below the convective coincidence frequency, the TBL excitation results in a more spatially correlated pressure field and re-creating this condition presents its difficulties. The wave field synthesis (Berry *et al.*, 2012) and the planar-near field acoustic holography (Robin *et al.*, 2013) are both methods that want to reproduce the TBL excitation through acoustic sources, respecting the TBL correlation scales. The first one can easily reproduce an acoustic plane wave and a diffuse acoustic field, but the same cannot be said for the TBL itself (Robin *et al.*, 2014). The second one is focused on the realisation of subsonic and supersonic TBL excitation, where the main difference consists of how many acoustic sources are to be considered for the array; while the supersonic case is easy to reproduce, the subsonic one is bound to the number of used monopoles in order to reproduce a faithful convective wavelength (Robin *et al.*, 2015).

In this work, the experimental application development of the pseudo-equivalent deterministic excitation method (PEDE_M) (De Rosa *et al.*, 2015) is carried on. Indeed, PEDE_M takes the main concept of modal decomposition applied from the pseudo excitation method (PEM) (Wilson *et al.*, 1981), individuating eigenvectors and eigenvalues of the load CSD matrix, and bypassing the actual modal computation by considering two asymptotic representations of the TBL CSD matrix eigensolutions—in low frequency (LF) and high frequency (HF) domains. The experimental application of PEDE_M (X-PEDE_M) in a HF domain has already been presented and validated numerically (Mazzeo *et al.*, 2022); with this new production, the extension of the method in the LF domain is presented, reaching a frequency-broadband prediction of the structural response to a TBL excitation.

In Sec. II, a brief theoretical background of PEDE_M is provided, in order to ensure a better comprehension of X-PEDE_M and its new formulation for LF domain application (Sec. III), followed by its main characteristics. Then, a numerical validation of the method is presented, giving a direct comparison between the numerical full stochastic response (FSR) obtained with different TBL models and X-PEDE_M, for different sample panels, different boundary conditions, and different flow velocities, in order to guarantee the versatility of the method (Sec. IV). In the last Sec. V, main remarks and open issues of the methodology are discussed.

II. PEDE_M THEORETICAL BACKGROUND

As previously stated, PEDE_M wants to provide a simpler formulation for the numerical structural response to a TBL excitation. Starting from the numerical FSR presented as a CSD displacement matrix $[S_{WW}(\omega)]$ in Eq. (1),

$$[S_{WW}(\omega)] = [\Phi][H(\omega)][\Phi]^T [S_{FF}(\omega)][\Phi][H^*(\omega)][\Phi]^T, \quad (1)$$

where $[\Phi]$ is the structural modal matrix, consisting of NG (number of grid points) structural degrees of freedom and NM (number of modes) $[NG \times NM]$; $[H(\omega)]$ is the structural transfer function diagonal matrix $[NM \times NM]$, for which each element of the diagonal is expressed as $H_m(\omega) = [\omega_m^2(1 + \eta_m) - \omega^2]^{-1}$; $[S_{FF}(\omega)]$ is the equivalent force matrix $[NG \times NG]$. The FSR solution is rewritten by considering the PEM and its modal decomposition (Wilson *et al.*, 1981) of the equivalent force CSD matrix

$$[S_{FF}(\omega)] = \sum_{i=1}^{NG} d_i(\omega) \{\Theta^{(i)}\} \{\Theta^{(i)}\}^T, \quad (2)$$

and considering the following expressions for the displacement vector and CSD displacement matrix

$$\{w(\omega, i)\} = [\Phi][H(\omega)][\Phi]^T \{\Theta^{(i)}\} \sqrt{d_i(\omega)}, \quad (3)$$

$$[S_{WW}(\omega)] = \sum_{i=1}^{NG} \{w^*(\omega, i)\} \{w^T(\omega, i)\}. \quad (4)$$

PEDE_M presents two different formulation of load eigenvectors $\{\Theta^{(i)}\}$ and eigenvalues $d_i(\omega)$, depending on the dimensionless frequency $\kappa = \omega\Delta/U_c$ (with ω as frequency, Δ as mesh size, and U_c as convective flow velocity):

- For $\kappa \rightarrow 0$, the spatial correlation is *totally correlated* (Franco *et al.*, 2013); hence, the eigenvector matrix $[\Theta]$ can be expressed with an all-1 matrix

$$[\Theta] = \begin{bmatrix} 1 & 1 & \dots & 1 \\ 1 & 1 & \dots & 1 \\ \vdots & \vdots & \ddots & \vdots \\ 1 & 1 & \dots & 1 \end{bmatrix}, \quad (5)$$

where the i th column of $[\Theta]$ is representative of the i th eigenvector of the load matrix. Only the first eigenvalue $d_{1,LF}$ will be non-null.

- For $\kappa \rightarrow \infty$, the spatial correlation is *totally uncorrelated*, which is relative to a Rain-On-the-Roof excitation (Ichchou *et al.*, 2015); a totally uncorrelation is expressed with an eigenvector matrix form as

$$[\Theta] = \begin{bmatrix} 1 & 0 & 0 & \dots & 0 \\ 0 & 1 & 0 & \dots & 0 \\ 0 & 0 & \ddots & \dots & \vdots \\ \vdots & \vdots & \vdots & \ddots & 0 \\ 0 & 0 & \dots & 0 & 1 \end{bmatrix}. \quad (6)$$

All eigenvalues are equal to the same value d_{HF} .

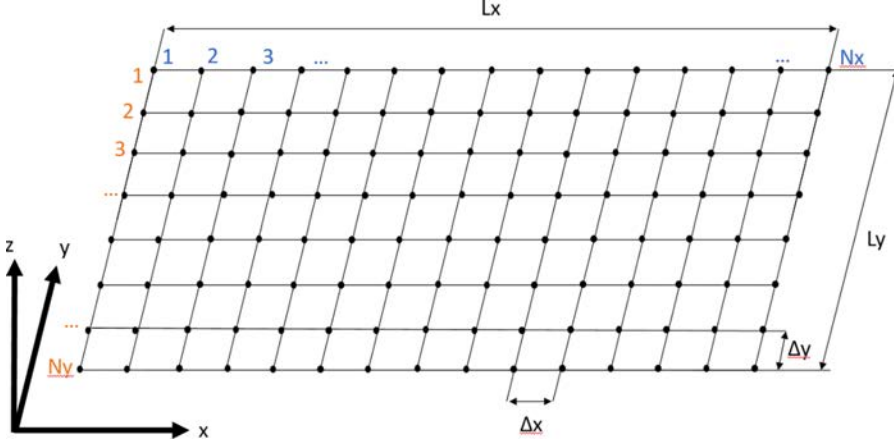


FIG. 1. (Color online) Example of mesh grid for a 2D-system as a plate.

It is important to provide some remarks about the aforementioned methods. Since the PEM is based on the modal decomposition of the load matrix, its application for the reproduction of the structural response will give a solution that inevitably converges to the FSR response. As a consequence, using PEDE_M for the same task also would ensure the convergence, due to the chosen asymptotic formulations. The X-PEDE_M wants to use the same PEDE_M formulation and apply it for experimental purposes based on the experimental acquisition of the frequency response functions (FRFs) of the structure under analysis. In Mazzeo *et al.* (2022), it has been demonstrated numerically that this experimental approach can be executed by using the PEDE_M formulation in the HF domain and it can reproduce, with a degree of approximation, the vibrational response of a structure subjected to a TBL excitation.

In the next section, the same attempt is explained, this time by using the PEDE_M formulation in the LF domain. By doing that, X-PEDE_M would be based on both asymptotic formulations; hence, it can be used to reproduce the structural response to a TBL excitation in a broadband frequency domain.

III. PEDE_M AND X-PEDE_M FORMULATION FOR LOW FREQUENCY DOMAIN

A. Eigenvalue formulation for PEDE_M in the LF domain

In De Rosa *et al.* (2015), PEDE_M was first introduced by analysing the structural response to a TBL excitation reproduced for a one-dimensional (1D) system consisting of $NG = 10$ oscillators in row. The TBL excitation model invoked for that analysis was the Corcos model (Corcos, 1963). The first and only non-null eigenvalue valid for the PEDE_M asymptotic behaviour in the LF domain was equal to NG .

In the case of a two-dimensional (2D) system, one can consider as example a plate with dimensions $L_x \times L_y$, for which its single finite element has dimensions $\Delta_x \times \Delta_y$ (Fig. 1). The number of grid points that make up the mesh of the panel is $NG = N_x \times N_y$.

As for the 1D-case, the Corcos model formulation [Eq. (7)] is chosen as representation of the TBL-induced pressure field, since it can well describe the spatial correlation in terms of distance between points over the structural surface (Fig. 2). In Eq. (7), it is possible to recognise the decay coefficients along the streamwise (α_x) and spanwise (α_y) direction and the convective flow velocity U_c related to the asymptotic flow velocity U_∞ through the convective coefficient $\beta_c = U_c/U_\infty$:

$$\Gamma_{pp}^{Corcos}(\zeta_x, \zeta_y; \omega) = (\Delta x \Delta y)^2 \exp\left(-\alpha_x \frac{\omega}{U_c} |\zeta_x|\right) \times \exp\left(-\alpha_y \frac{\omega}{U_c} |\zeta_y|\right) \exp\left(i \frac{\omega}{U_c} \zeta_x\right). \quad (7)$$

For finite elements with dimensions $\Delta_x = \Delta_y = \Delta$, the distances between the coordinates points along the x -direction and y -direction can be expressed, respectively

$$\zeta_x = (n_x - 1)\Delta \quad \text{with } n_x = 1, 2, \dots, N_x, \quad (8a)$$

$$\zeta_y = (n_y - 1)\Delta \quad \text{with } n_y = 1, 2, \dots, N_y. \quad (8b)$$

With these premises, it is easy to evaluate the TBL excitation behaviour when the dimensionless frequency $\kappa = \omega\Delta/U_c$ tends to zero:

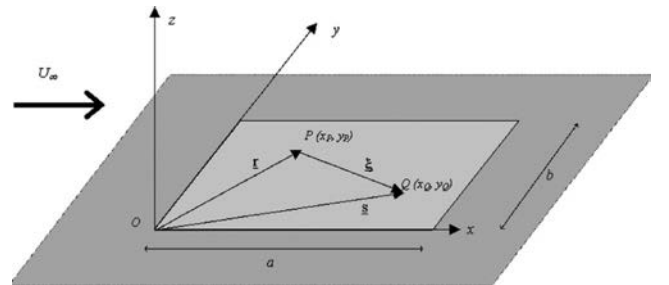


FIG. 2. Representation of a plate subjected to an air flow of asymptotic velocity U_∞ ; two points are represented to stress the dependence that 2-points spectra excitation models have on the distance between them.

$$\lim_{\kappa \rightarrow 0} \Gamma_{pp'}^{Corcos}(\zeta_x, \zeta_y; \omega) = \Delta^2. \quad (9)$$

By observing other WPFs expressions, as the Mellen model (Mellen, 1990) and the incident diffuse field (IDF) (De Rosa and Franco, 2008),

$$\begin{aligned} \Gamma_{pp'}^{Mellen}(\zeta_x, \zeta_y; \omega) \\ = (\Delta x \Delta y)^2 \exp \left[\left[\left(\alpha_x \frac{\omega}{U_c} \zeta_x \right)^2 + \left(\alpha_y \frac{\omega}{U_c} \zeta_y \right)^2 \right]^{1/2} \right] \\ \times \exp \left[i \frac{\omega}{U_c} \zeta_x \right], \end{aligned} \quad (10)$$

$$\Gamma_{pp'}^{IDF}(\zeta_x, \zeta_y; \omega) = (\Delta x \Delta y)^2 \frac{\sin(\omega \zeta_x / U_c)}{\omega \zeta_x / U_c} \frac{\sin(\omega \zeta_y / U_c)}{\omega \zeta_y / U_c}, \quad (11)$$

it is possible to recognise that, when their behaviour is studied for $\kappa \rightarrow 0$, their limit is equal to the squared value of the finite element area Δ^2 .

This is true when the limit is applied to each element of the CSD load matrix built with one of the three aforementioned WPFs formulation. Hence, it is assumed that the first and only non-null eigenvalue for PEDE_M in the LF domain is equal to $d_{1,LF} = \Delta^2$.

B. X-PEDE_M formulation for LF domain

The experimental application of PEDEM in the low frequency domain is based on the acquisition of the FRFs characteristic of a structure, as it is X-PEDE_M for high frequency domain applications (Mazzeo *et al.*, 2022). The main differences between the processes for the prediction in low and high frequency domain lie on: (1) the excitation points position, which is not randomly chosen anymore, and (2) the post-processing data phase.

From a mathematical point of view, X-PEDE_M starts with Eq. (3), representing the i th displacement vector, where i counts the number of eigensolutions resulted from the load matrix modal decomposition. It is important to remark on two main aspects of this formula when it is applied for HF domain applications:

- All eigenvectors $\{\Theta^{(i)}\}$ are part of an identity matrix; this represents the totally spatial uncorrelation among excitation points. Consequently, the evaluation of one CSD displacement matrix is evaluated for a single excitation point.
- All eigenvalues $d_i(\omega)$ are different from zero and equal to each other; this represents the superposition of effects for which the CSD displacement matrix is evaluated for each different excitation point and the actual solution is the result of a sum of all CSD matrices evaluated for each chosen excitation point [Eq. (4)].

When Eq. (3) is applied for LF domain applications, eigenvectors and eigenvalue are different (as previously

defined in Sec. II); hence, they involve a different evaluation of the CSD displacement matrix and the displacement vector $\{w(\omega)\}$. First, it is noticed that the displacement vector $\{w(\omega)\}$ is calculated only one time, since there is only one non-null eigenvalue; consequently, the CSD displacement matrix is evaluated only one time, too. Second, one can reconsider the matrix product expressed in Eq. (3) by individuating the matrix $[S_\phi]$ [Eq. (12a)] and its generic element $S_{\phi(j,i)}$ [Eq. (12b)]:

$$[S_\phi] = [\Phi][H(\omega)][\Phi^T], \quad (12a)$$

$$S_{\phi(j,i)} = \sum_m \Phi_{j,m} H_{m,m} \Phi_{m,i}. \quad (12b)$$

Multiplying any matrix by an all-1 vector results in a column vector in which each element is the sum of each matrix row. Therefore, one can interpret the single displacement element $w_j(\omega)$ measured in the j th acquisition point as

$$w_j(\omega) = \sum_{i=1}^{N_{ex}} \sum_m \frac{\phi_m(P_j) \phi_m(P_i) F_m^{(i)}}{h_m(\omega)}, \quad (13)$$

where $F_m^{(i)} = \sqrt{d_{1,LF}}$. It is important to remark that $d_{1,LF} = \Delta^2 = L_x L_y / NG$, as it is equal to the square value of the finite element area. This is valid when the model applied is $\text{PEDE}_{M,LF}$, which considers, as excitation points, all the points of the mesh grid, $N_{ex} = NG$. With X-PEDE_{M,LF}, on the other hand, the equivalent finite element area A_{ex} is considered, which is related to the number of excitation points considered,

$$d_{1,LF} = A_{ex}^2 = \left(\frac{L_x L_y}{N_{ex}} \right)^2. \quad (14)$$

From a physical point of view, the displacement in each acquisition point is evaluated as if all the N_{ex} excitation points are excited simultaneously. The modal force factor $F_m^{(i)}$ does not depend on either the modes or the excitation points position; hence, it is enough to evaluate the FRFs between each acquisition and all excitation points, sum them, and post-process the value with the corrective factor $\sqrt{d_{1,LF}}$,

$$w_j(\omega) = \sqrt{d_{1,LF}} \sum_{i=1}^{N_{ex}} \sum_m \frac{\phi_m(P_j) \phi_m(P_i)}{h_m(\omega)}. \quad (15)$$

From an experimental point of view, the application of X-PEDE_{M,LF} is divided in two main phases: the collecting experimental data and the post-processing data phase, as it is for the application of X-PEDE_M applied in the HF domain (X-PEDE_{M,HF}). The experiment phase can be performed with a hammer test and it goes as follows:

- (1) Subdivide the structure in discrete elements, defining a mesh grid.

- (2) Arrange the accelerometers in the chosen acquisition points positions.
- (3) Select the excitation points.
- (4) Excite the structure in one excitation point at the time, registering the structural response in terms of FRFs in all the acquisition points.

The post-processing data phase is developed by following the next steps:

- (1) Organise the experimental data set by grouping all the FRFs relating to each acquisition point, obtaining N_{acq} groups of FRFs.
- (2) For each acquisition point, sum all the FRFs and then multiply by the force corrective factor $\sqrt{d_{1,LF}}$, obtaining the displacement defined in Eq. (15).
- (3) Save all the displacements in the displacement vector $\{w(\omega)\}$, of dimensions $[N_{acq} \times 1]$.
- (4) Calculate the CSD displacement matrix as

$$[S_{WW}(\omega)] = \{w^*(\omega)\}\{w^T(\omega)\}. \quad (16)$$

- (5) Evaluate the mean PSD displacement as

$$\bar{S}_{ww}(\omega) = \frac{1}{N_{acq}} \sum_{j=1}^{N_{acq}} [S_{WW}(\omega)]_{(j,j)}. \quad (17)$$

The selection of excitation and acquisition points cannot be done randomly as it is for X-PEDE_{M_{HF}}, but once the selection is done for the application of X-PEDE_{M_{LF}}, the same experimental data can be used for both the post-processing phases of X-PEDE_{M_{LF}} and X-PEDE_{M_{HF}}. In the following subsection, the selection of excitation and acquisition points is discussed.

C. X-PEDE_M points selection process

1. Position of excitation points

In the HF domain, the PEDE_M formulation is based on the assumption of a totally uncorrelated spatial distribution of the WPFs; hence, X-PEDE_{M_{HF}} does not depend on the choice of excitation and acquisition points positions, but just on their number. It has been seen that at least 5 acquisition points and 10 excitation points, with random position, are needed to ensure a good reproduction of the solution. On the other hand, in the LF domain, PEDE_M is based on the assumption of a totally correlated spatial distribution; hence, the choice of excitation and acquisition points position can indeed affect the prediction of the response. In order to determine for which group of points it is important to know their position, a trial and error process has been conducted.

For this trial and error process, a sample aluminium panel with simply-supported boundary conditions is here considered (geometry and material properties in Table I). As TBL excitation, the Corcos model is invoked, by fixing the asymptotic flow velocity at $U_\infty = 200$ m/s and the

TABLE I. Sample panel information for the trial and error process for the determination of number and position of excitation and acquisition points.

First sample panel information		
Geometry	Material	Mesh
$L_x = 0.201$ m	$E = 6.89 \times 10^{10}$ Pa	$N_x = 28$
$L_y = 0.120$ m	$\rho = 2700$ kg/m ³	$N_y = 17$
$h = 0.0015$ m	$\nu = 0.30$	$NG = 476$
Boundary conditions: simply supported		

following empirical coefficients as $\alpha_x = 0.116$, $\alpha_y = 0.700$, and $\beta_c = 0.80$.

As the first phase, the excitation points position are determined by keeping fixed, as acquisition points, all the grid points. In Fig. 3, the analytical solution is compared with the X-PEDE_{M_{LF}} for three different distributions of excitation points.

It is easy to notice that an equally distributed mesh of excitation points is not a good choice for the X-PEDE_{M_{LF}}. Whether it is fine [Fig. 3(a)] or coarse [Fig. 3(c)], the X-PEDE_{M_{LF}} is not able to represent all the structural modes in the response [respectively, Figs. 3(b) and 3(d)]. The same deduction can be done by keeping the number of excitation points comparable to the case presented in Fig. 3(c), but with a diagonally equal distribution of the excitation points [Figs. 3(e) and 3(f)].

Another set of excitation points distribution is then considered in Fig. 4. Single directions have been chosen in order to understand whether different excitation point line distributions can ensure different modal information in the structural response. Indeed, both vertical configuration of excitation points [Fig. 4(a)] and horizontal configuration of excitation points [Fig. 4(c)] can represent just some modes, but not all of them, and not the same [Figs. 4(b) and (d)]; the diagonal line distribution [Fig. 4(e)], on the other hand, can represent all the modes, but with some discrepancies [Fig. 4(f)].

Finally, the best configuration has been individuated by considering a combination of the three main directions previously presented. In Fig. 5, one can see that the comparison between X-PEDE_{M_{LF}} and an analytical solution is consistent, even when the number of excitation points is reduced. As it has been stated for X-PEDE_{M_{HF}}, a minimum number of 10 excitation points is suggested in order to ensure an optimal agreement between the solution and its reference.

A few guidelines are here summarised in order to find the optimal configuration of excitation points:

- (i) Individuate three main directions over the sample panel: two along its sides and the third going along the diagonal of the panel.
- (ii) A constant distance between each excitation point along each direction is suggested, but not mandatory. In any case, the length of the sides and diagonal length need to be covered.
- (iii) A minimum number of 10 excitation points is required for an optimal description of the structural response.

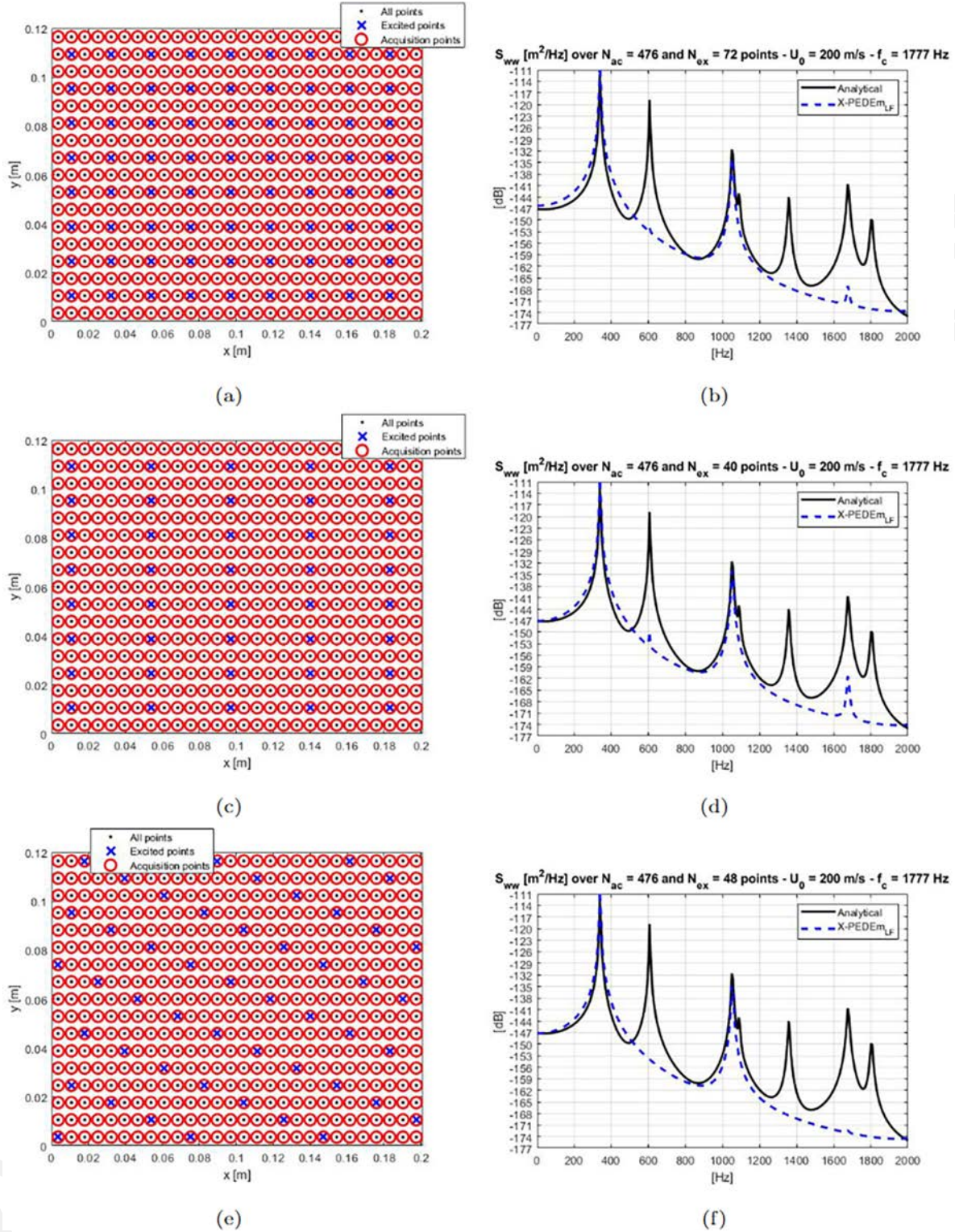


FIG. 3. (Color online) Comparison between analytical S_{ww} solution (solid black line) and X-PEDEm_{LF} S_{ww} solution (dashed blue line) for $U_\infty = 200$ m/s by keeping fixed the acquisition points. (a) and (b) Equal distribution of $N_{ex} = 72$ points, (c) and (d) equal distribution of $N_{ex} = 40$ points, (e) and (f) diagonal distribution of $N_{ex} = 48$ points.

2. Position of acquisition points

Once the optimal choice for number and position of excitation points has been found, a trial and error process has been performed for the acquisition points, even though, by definition of the problem in terms of totally correlated

spatial distribution of the excitation, it was expected that the number and position of acquisition points would not affect the solution as number and position of excitation points would do. Indeed, in Fig. 6, it is possible to appreciate the independence of the solution on the acquisition points

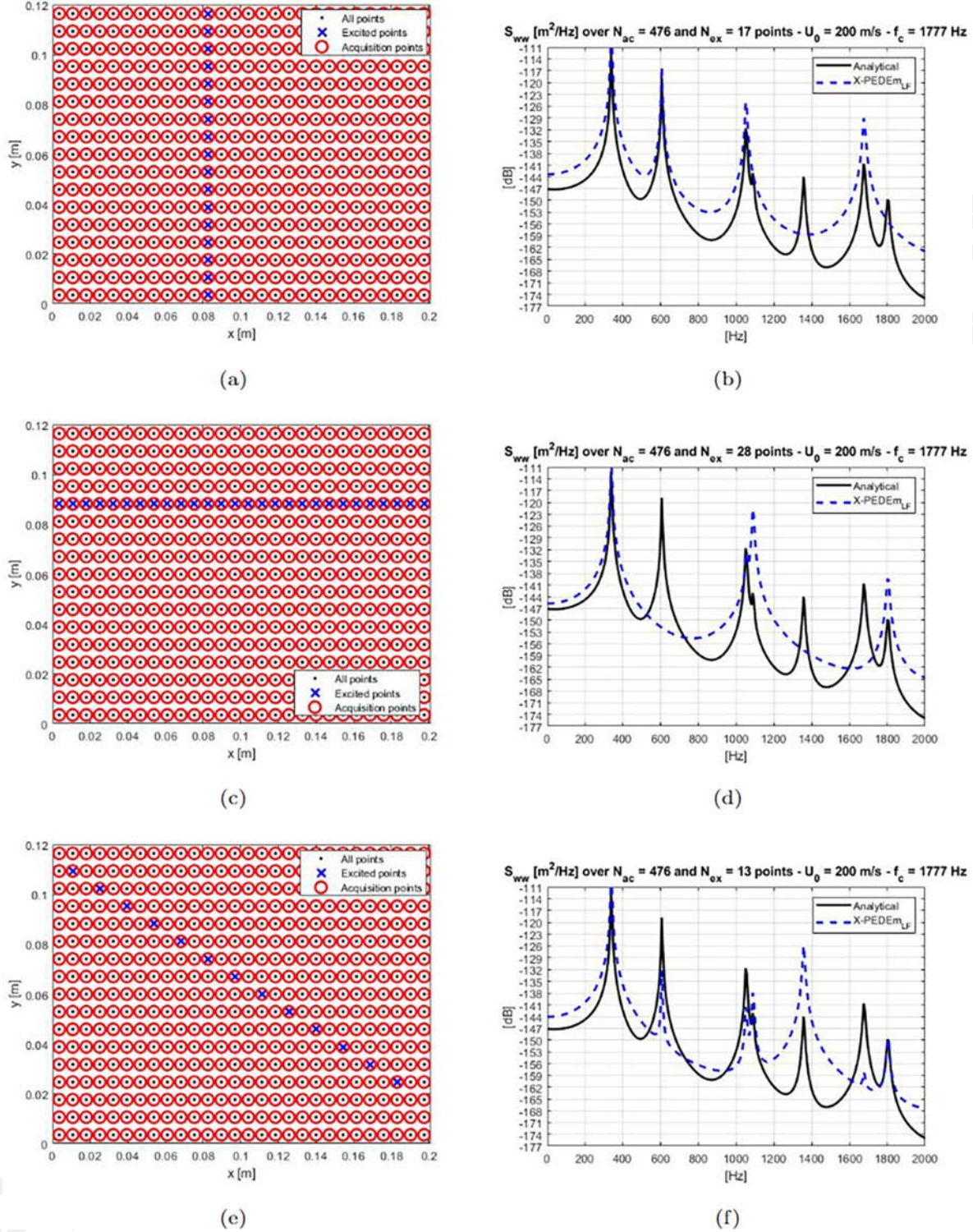


FIG. 4. (Color online) Comparison between analytical S_{ww} solution (solid black line) and X-PEDE $_{M_{LF}}$ S_{ww} solution (dashed blue line) for $U_{\infty} = 200$ m/s by keeping fixed the acquisition points. (a) and (b) single vertical line with $N_{ex} = 17$; (c) and (d) single horizontal line with $N_{ex} = 28$; (e) and (f) single diagonal line with $N_{ex} = 13$.

configuration, which can be chosen randomly and just assuring a minimum number of 5 acquisition points for a better reproduction of the solution.

Figure 6(f) can be a first validation of the method, since it shows the analytical structural response of a panel, with simply supported boundary conditions, excited by a TBL

excitation expressed through the Corcos model, in comparison with the X-PEDE $_{M_{LF}}$ solution, estimated with $N_{ex} = 28$ excitation points and $N_{acq} = 7$ acquisition points—the last ones randomly chosen. The comparison is optimal until a certain frequency in proximity of the convective coincidence frequency f_c ; which, for this particular case of an

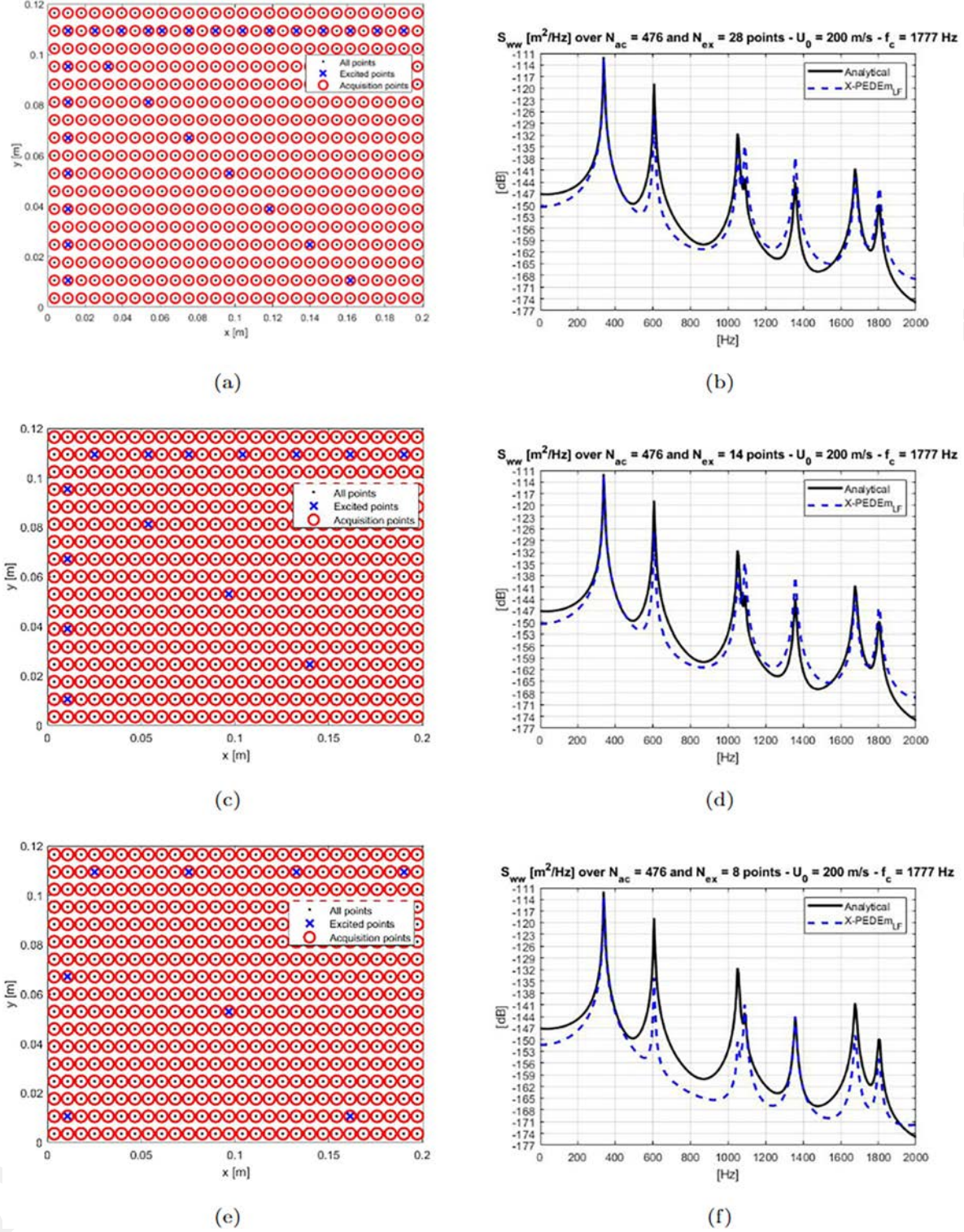


FIG. 5. (Color online) Comparison between analytical S_{ww} solution (solid black line) and X-PEDE_{MLF} S_{ww} solution (dashed blue line) for $U_\infty = 200$ m/s by keeping fixed the acquisition points. (a) and (b) Best excitation points configuration with $N_{ex} = 28$, (c) and (d) best excitation points configuration with $N_{ex} = 14$, (e) and (f) best excitation points configuration with $N_{ex} = 8$.

asymptotic flow velocity of $U_\infty = 200$ m/s, is equal to $f_c = 1777$ Hz.

To assess the robustness of the method in function of the unavoidable errors due to points selections for acquisition and excitation, a mean percentage error has been

evaluated. By keeping a fixed number and position of acquisition points ($N_{acq}=8$), 20 sample X-PEDE_{MLF} solutions are calculated, for which the number of excitation points is fixed $N_{ex}=27$, but the positions along the three main directions are chosen randomly. This strategy wants to simulate the

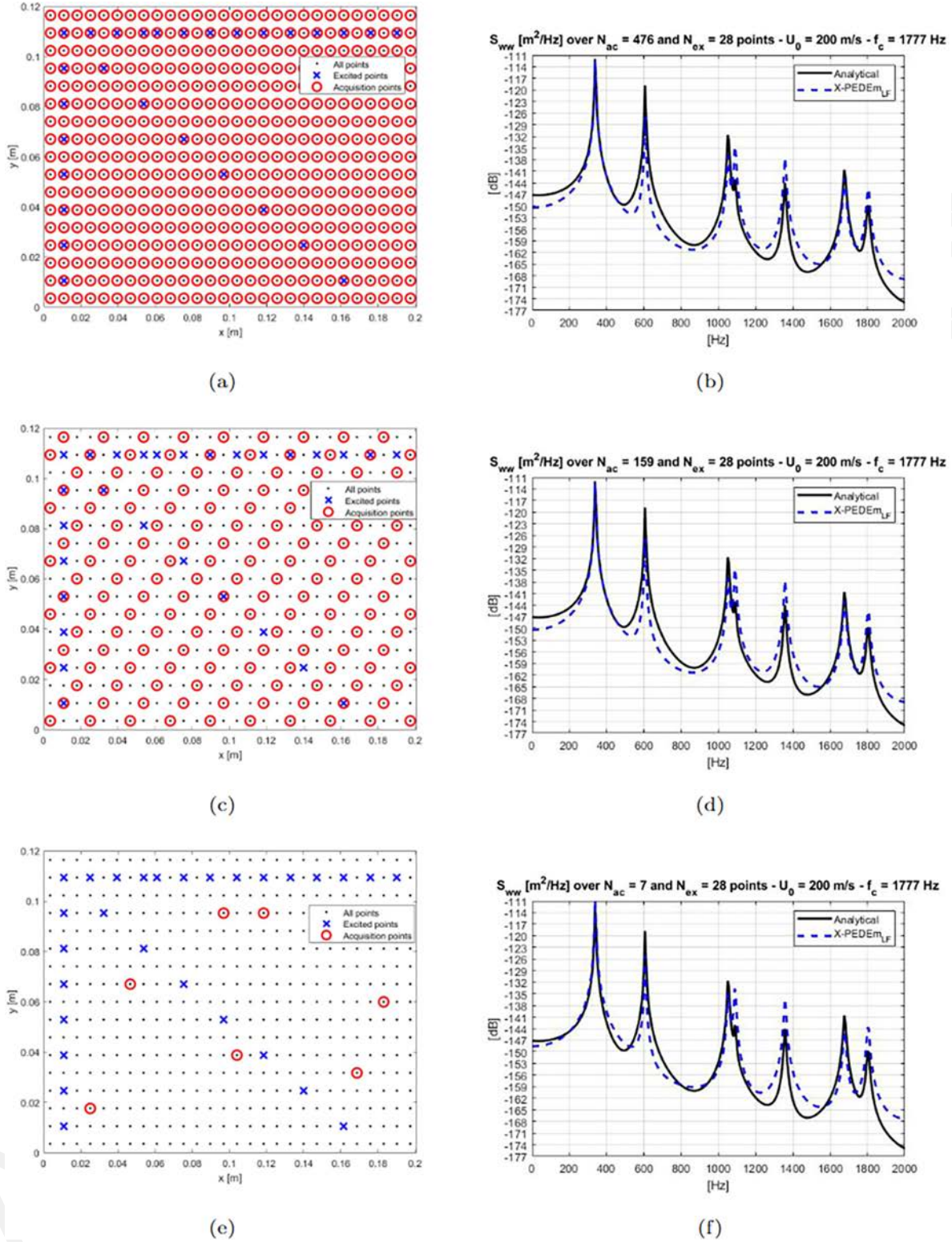


FIG. 6. (Color online) Comparison between analytical S_{ww} solution (solid black line) and X-PEDE $_{MLF}$ S_{ww} solution (dashed blue line) for $U_\infty = 200$ m/s by keeping fixed the excitation points number and position. (a) and (b) All acquisition points $N_{acq} = 476$, (c) and (d) $\frac{1}{3}$ of acquisition points ($N_{acq} = 159$), equally distributed, (e) and (f) random choice of $N_{acq} = 7$ acquisition points.

error in positioning an actuator over the structure. In Fig. 7, all 20 sample solutions of the PSD acceleration of a sample panel (Table I) are shown in gray, together with the target X-PEDE $_{MLF}$ solution in red.

The percentage error of each sample solution is evaluated in function of the target X-PEDE $_{MLF}$ solution and then a mean percentage error is estimated. It is possible to notice that the percentage error is very low in the low frequency

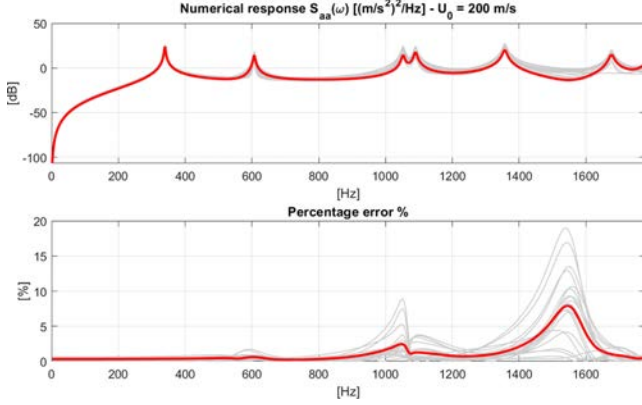


FIG. 7. (Color online) Top: 20 sample X-PEDE_{MLF} solutions (gray lines) estimated for different excitation points positions in comparison with the target X-PEDE_{MLF} solution (red line) for which all excitation points are well located. Bottom: percentage error of each sample solution (gray lines) and the mean percentage error (red line).

domain and tends to increase when the solutions reach the coincidence convective frequency ($f_c = 1777$ Hz), as expected by the methodology. Nevertheless, the mean percentage error does not overpass the 8%, demonstrating a robustness to location errors.

X-PEDE_{MLF} proves to be an interesting tool that is not a substitute for the accuracy of a wind tunnel facility, but it can give a prediction on how to obtain an optimal setup in a wind tunnel. Moreover, it can be used to estimate *a priori* the percentage error that the actual experimental result might present.

More cases and insights are investigated in the following section.

IV. NUMERICAL VALIDATION OF X-PEDE_M APPLIED IN THE LF DOMAIN

In Fig. 8, the same panel presented in Table I is tested for the evaluation of its structural response under different WPFs models.

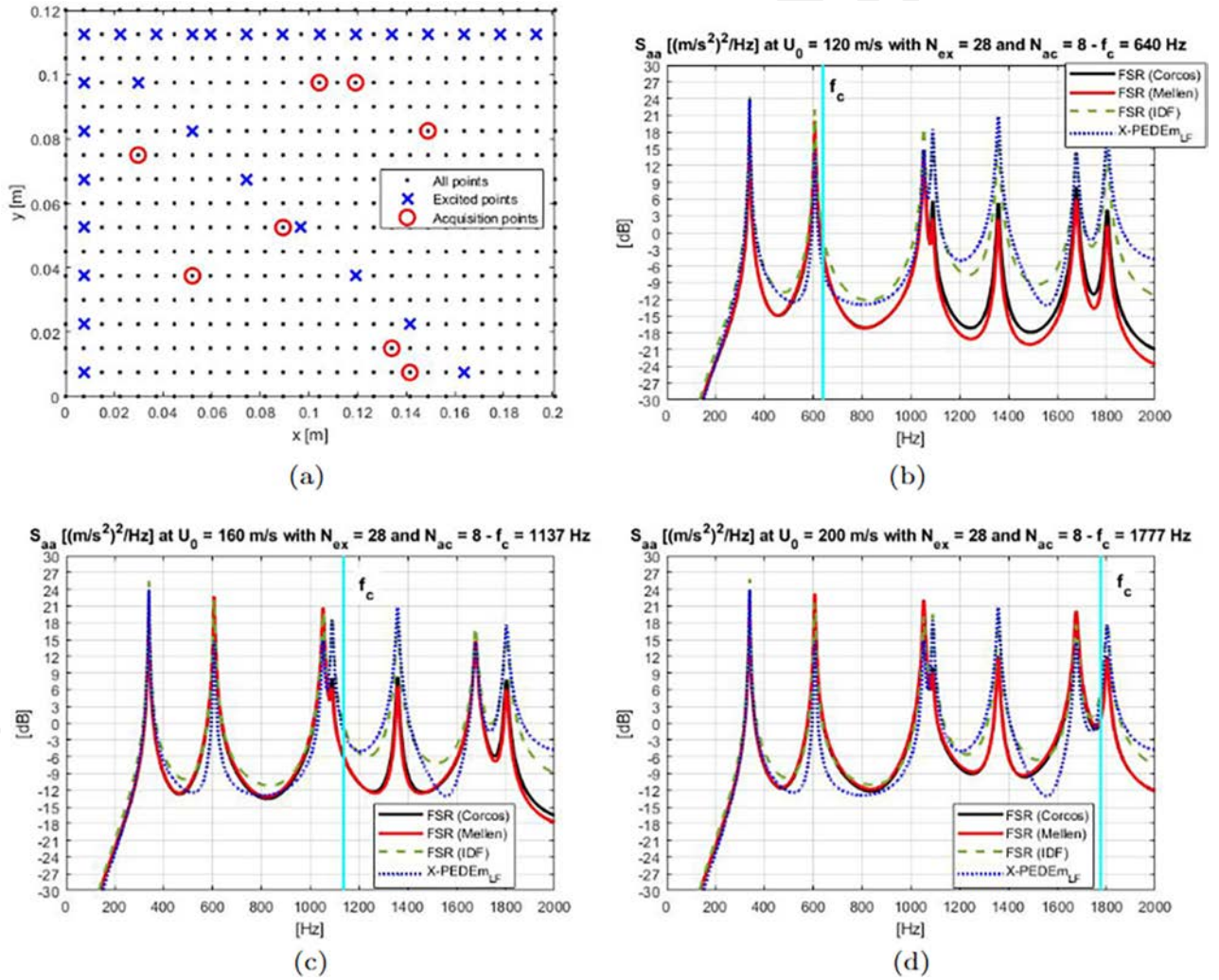


FIG. 8. (Color online) Comparison between X-PEDE_{MLF} solution (dotted blue line) and numerical FSR $S_{aa}(\omega)$ calculated with different WPFs models at different flow velocities: Corcos model (solid black line), Mellen model (solid red line), IDF (dashed green line). (a) Mesh grid with $N_{acq} = 7$ acquisition points randomly chosen (red circles) and $N_{ex} = 28$ excitation points (blue crosses), (b) comparison for $U_\infty = 120$ m/s, with $f_c = 640$ Hz, (c) comparison for $U_\infty = 160$ m/s, with $f_c = 1137$ Hz, (d) comparison for $U_\infty = 200$ m/s, with $f_c = 1777$ Hz.

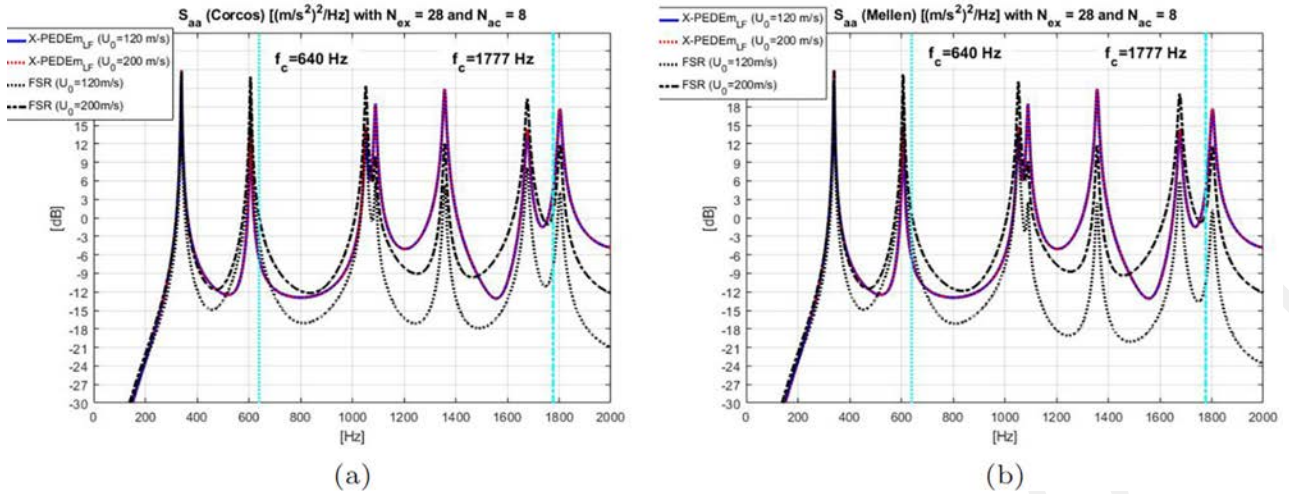


FIG. 9. (Color online) Comparison between X-PEDE_{MLF} solution and numerical FSR $S_{aa}(\omega)$ calculated at two different asymptotic flow velocities: FSR at $U_\infty = 200$ m/s (dot-dashed black line), FSR at $U_\infty = 120$ m/s (dotted black line), X-PEDE_{MLF} at $U_\infty = 200$ m/s (dotted red line), X-PEDE_{MLF} at $U_\infty = 120$ m/s (solid blue line). (a) FSR calculated with Corcos model, (b) FSR calculated with Mellen model.

This time, the reference solution is calculated as numerical FSR [Eq. (1)], since no analytical formulations involve the use of the Mellen model and the IDF model.

The X-PEDE_{MLF} solution is calculated for a different choice of acquisition points [Fig. 8(a)] and it is compared with these three WPFs models for three different asymptotic flow velocities: $U_\infty = 120$ m/s, presenting a $f_c = 640$ Hz [Fig. 8(b)], $U_\infty = 160$ with $f_c = 1137$ Hz [Fig. 8(c)], and $U_\infty = 200$ m/s with $f_c = 1777$ Hz [Fig. 8(d)]. It can be noticed that X-PEDE_{MLF} can reproduce the response for different acquisition points—validating the possibility of randomly choosing their position—and for different asymptotic flow velocities, up to a frequency in proximity of the convective coincidence frequency f_c .

As for X-PEDE_{MHF}, the convective coincidence frequency is here indicated as *approximated* frequency limit in order to define the point at which frequency the method is valid. Considering the general X-PEDE_M methodology, one can apply the X-PEDE_{MLF} in a frequency region below f_c and then the X-PEDE_{MHF} in a frequency region above f_c . Although it can be said that f_c is valid for TBL excitation models, such as Corcos and Mellen, the same cannot be said for the IDF model, since the FSR seems to be well reproduced, even above the f_c limit.

Through the expression of the displacement in Eq. (15), it is evident that the application of X-PEDE_M in the LF

domain is independent on the flow velocity U_∞ , differently from the case in the HF domain, where different eigenvalue formulations $d_{i,HF}(\omega)$ can be used in order to better reproduce the structural response to a TBL excitation, depending on the type of excitation model adopted (Mazzeo *et al.*, 2022).

The independence of X-PEDE_{MLF} is well represented in Fig. 9, where the method is applied for two different flow velocities— $U_\infty = 120$ m/s and $U_\infty = 200$ m/s, and the solutions are perfectly identical, both for the Corcos model [Fig. 9(a)] and the Mellen model [Fig. 9(b)]. As a matter of fact, one can turn the comparison upside down by keeping the X-PEDE_{MLF} as reference and notice how the FSRs diverge from it, depending on which U_∞ is considered, since the divergence happens around the convective coincidence frequency.

TABLE II. Sample panel information for the X-PEDE_M validation.

Second sample panel information		
Geometry	Material	Mesh
$L_x = 0.480$ m	$E = 7.10e10$ Pa	$N_x = 48$
$L_y = 0.660$ m	$\rho = 2700$ kg/m ³	$N_y = 66$
$h = 0.0030$ m	$\nu = 0.33$	$NG = 3168$
Boundary conditions: all free edges		

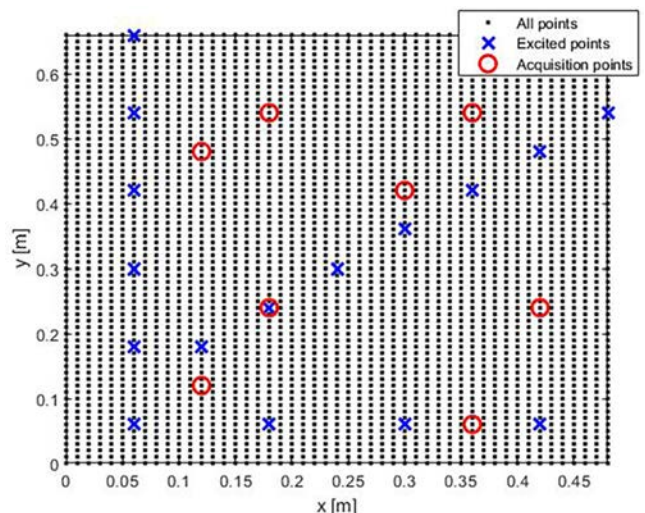


FIG. 10. (Color online) Mesh grid of the second sample panel. Selected excitation points (blue crosses), selected acquisition points (red circles).

For a last validation of the presented method, an aluminium panel with totally free boundary conditions has been tested; material and geometry properties are reported in Table II. The mesh grid, with the selection of excitation and acquisition points, is shown in Fig. 10.

The numerical FSR is evaluated for both the Corcos and Mellen model at three different asymptotic flow velocities: $U_\infty = [25 \ 75 \ 125]$ m/s and a comparison with X-PEDE $_M$, both for low and high frequency domain application (shown in Fig. 11).

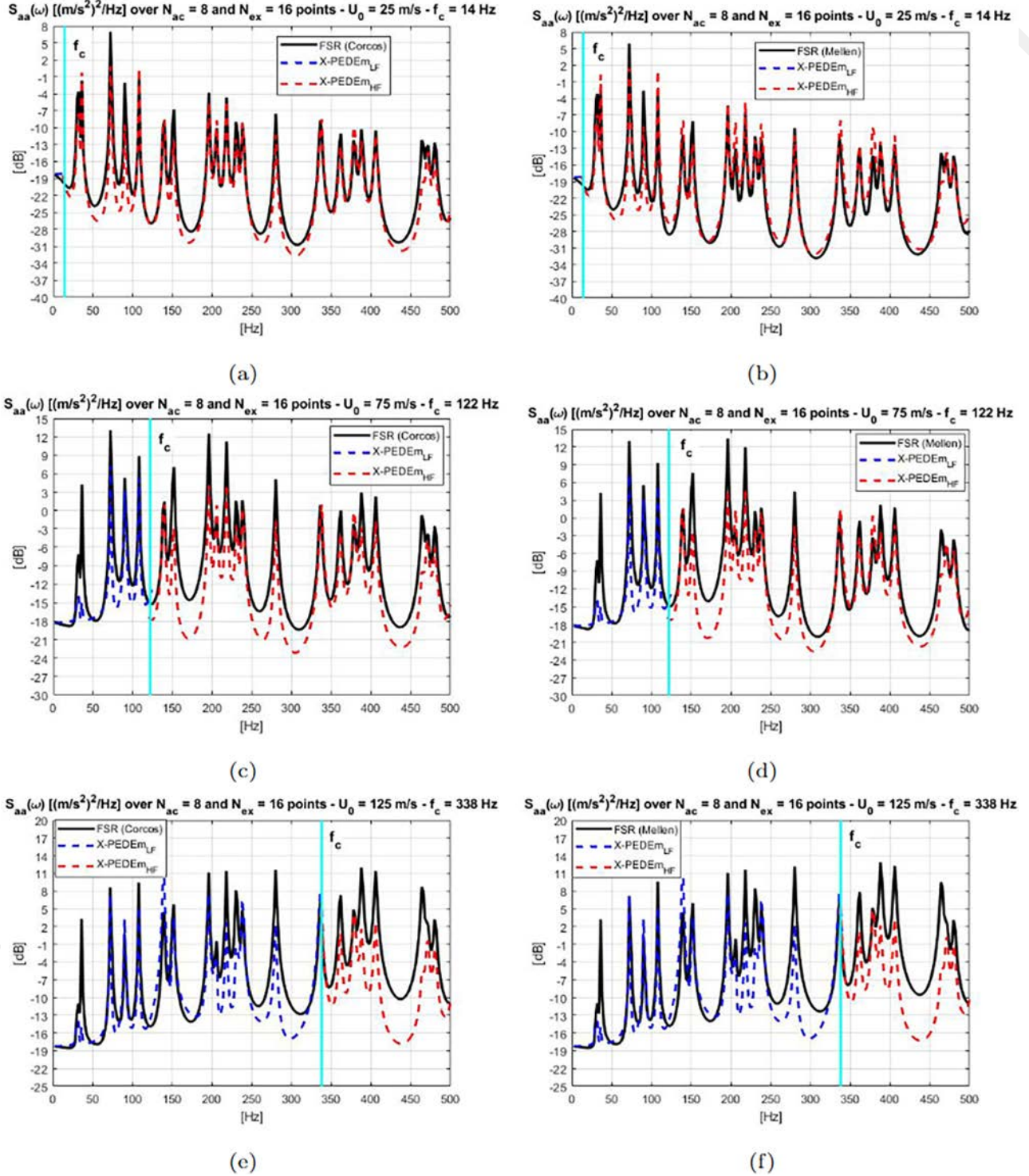


FIG. 11. (Color online) Comparison between the numerical FSR (solid black line) and X-PEDE $_M$ applied in the LF domain (dashed blue line) and HF domain (dashed red line) for different asymptotic flow velocities. (a) Corcos model at $U_\infty = 25$ m/s, (b) Mellen model at $U_\infty = 25$ m/s, (c) Corcos model at $U_\infty = 75$ m/s, (d) Mellen model at $U_\infty = 75$ m/s, (e) Corcos model at $U_\infty = 125$ m/s, (f) Mellen model at $U_\infty = 125$ m/s.

Both of the methodologies can reproduce the structural response to an aerodynamic load expressed as TBL excitation, covering all the frequency region of interest, consisting of the sub-convective and super-convective regions. It is once again emphasised that the convective coincidence frequency is here used as an approximated indicator of the frequency limit for the X-PEDE_M application. Indeed, around this frequency, it is visible that both methods lose accuracy in the prediction of the response. The method, in its entirety, presents a computational cost on the order of seconds, while the numerical FSR takes hours to compute.

Even from an experimental point of view, the experimental setup of a hammer test requires much less time and complexity if compared to the one performed in a wind tunnel facility.

V. CONCLUSIONS

The intention of this work is to present an alternative methodology that can provide the structural response to a TBL excitation in an approximated way, but with a very low computational cost, in order to have fast predictive data useful for pre-design purposes and to accelerate an analysis process.

The X-PEDE_M has been here extended to the low frequency domain; the full process of collecting data and post-processing data has been given in detail. Then, main characteristics of the method have been assessed in order to allow a better comprehension of the presented formulations.

Finally, the method has been validated using various samples under different boundary conditions (all free edges and simply-supported edges) and at varying asymptotic flow velocities. It has, hence, been demonstrated the high versatility of the method, which is able now to cover a broadband frequency region and can operate under different TBL models.

Nevertheless, the development of X-PEDE_M is still ongoing, since there are several open issues to address:

- It is important to define the actual frequency limits of validation, since the convective coincidence frequency is just an approximated indicator. Finding the frequency limits for both X-PEDE_M formulations will also allow the determination of a middle frequency range where the extension of the method is required.
- An experimental application of the method is necessary in order to validate its experimental purpose.
- A final comparison between the experiments run in a wind tunnel facility and the X-PEDE_M experimental application is required.

ACKNOWLEDGMENTS

The authors thank the FEDER/FSE Rhône-Alpes for supporting this work under the framework of the collaborative project IJES.

AUTHOR DECLARATIONS

Conflict of Interest

The authors have no conflicts to disclose.

DATA AVAILABILITY

Data sharing is not applicable to this article as no new data were created or analyzed in this study.

NOMENCLATURE

CSD	Cross-spectral density
FEA	Finite element analysis
FRFs	Frequency response functions
FSR	Full stochastic response
HF	High frequency
IDF	Incident diffuse field
LF	Low frequency
PEDE _M	Pseudo-equivalent deterministic excitation method
PEDE _{MHF}	PEDE _M applied in the HF domain
PEDE _{MLF}	PEDE _M applied in the LF domain
PEM	Pseudo excitation method
PSD	Power spectral density
TBL	Turbulent boundary layer
UWPWs	Uncorrelated wall plane waves
WPFs	Wall-pressure fluctuations
X-PEDE _M	Experimental application of PEDE _M
X-PEDE _{MHF}	Experimental application of PEDE _M in the HF domain
X-PEDE _{MLF}	Experimental application of PEDE _M in the LF domain

Aucejo, M., Maxit, L., and Guyader, J.-L. (2012). "Experimental simulation of turbulent boundary layer induced vibrations by using a synthetic array," *J. Sound Vib.* **331**(16), 3824–3843.

Berry, A., Dia, R., and Robin, O. (2012). "A wave field synthesis approach to reproduction of spatially correlated sound fields," *J. Acoust. Soc. Am.* **131**(2), 1226–1239.

Bull, M. (1996). "Wall-pressure fluctuations beneath turbulent boundary layers: Some reflections on forty years of research," *J. Sound Vib.* **190**(3), 299–315.

Chase, D. M. (1980). "Modeling the wavevector-frequency spectrum of turbulent boundary layer wall pressure," *J. Sound Vib.* **70**(1), 29–67.

Corcos, G. (1963). "Resolution of pressure in turbulence," *J. Acoust. Soc. Am.* **35**(2), 192–199.

De Rosa, S., and Franco, F. (2008). "Exact and numerical responses of a plate under a turbulent boundary layer excitation," *J. Fluids Struct.* **24**(2), 212–230.

De Rosa, S., Franco, F., and Ciappi, E. (2015). "A simplified method for the analysis of the stochastic response in discrete coordinates," *J. Sound Vib.* **339**, 359–375.

Fahy, F. (1966). "On simulating the transmission through structures of noise from turbulent boundary layer pressure fluctuations," *J. Sound Vib.* **3**(1), 57–81.

Franco, F., De Rosa, S., and Ciappi, E. (2013). "Numerical approximations on the predictive responses of plates under stochastic and convective loads," *J. Fluids Struct.* **42**, 296–312.

Goody, M. (2004). "Empirical spectral model of surface pressure fluctuations," *AIAA J.* **42**(9), 1788–1794.

Hambric, S., and Lysak, P. (2019). "Validation of a simple empirical model for calculating the vibration of flat plates excited by incompressible

- homogeneous turbulent boundary layer flow,” in *International Conference on Flow Induced Noise and Vibration Issues and Aspects* (Springer, Berlin), pp. 61–85.
- Ichchou, M. N., Bareille, O., Troclet, B., Hiverniau, B., De Rochambeau, M., and Chronopoulos, D. (2015). “Vibroacoustics under aerodynamic excitations,” in *International Conference on Flow Induced Noise and Vibration Issues and Aspects* (Springer, Berlin), pp. 227–247.
- Karimi, M., Croaker, P., Maxit, L., Robin, O., Skvortsov, A., Marburg, S., and Kessissoglou, N. (2020). “A hybrid numerical approach to predict the vibrational responses of panels excited by a turbulent boundary layer,” *J. Fluids Struct.* **92**, 102814.
- Karimi, M., Croaker, P., Skvortsov, A., Maxit, L., and Kirby, R. (2021). “Simulation of airfoil surface pressure due to incident turbulence using realizations of uncorrelated wall plane waves,” *J. Acoust. Soc. Am.* **149**(2), 1085–1096.
- Marchetto, C., Maxit, L., Robin, O., and Berry, A. (2017). “Vibroacoustic response of panels under diffuse acoustic field excitation from sensitivity functions and reciprocity principles,” *J. Acoust. Soc. Am.* **141**(6), 4508–4521.
- Marchetto, C., Maxit, L., Robin, O., and Berry, A. (2018). “Experimental prediction of the vibration response of panels under a turbulent boundary layer excitation from sensitivity functions,” *J. Acoust. Soc. Am.* **143**(5), 2954–2964.
- Maury, C., Elliott, S. J., and Gardonio, P. (2004). “Turbulent boundary-layer simulation with an array of loudspeakers,” *AIAA J.* **42**(4), 706–713.
- Mazzeo, G., Ichchou, M., Petrone, G., Bareille, O., De Rosa, S., and Franco, F. (2022). “Pseudo-equivalent deterministic excitation method application for experimental reproduction of a structural response to a turbulent boundary layer excitation,” *J. Acoust. Soc. Am.* **152**(3), 1498–1514.
- Mellen, R. H. (1990). “On modeling convective turbulence,” *J. Acoust. Soc. Am.* **88**(6), 2891–2893.
- Robin, O., Berry, A., and Moreau, S. (2013). “Reproduction of random pressure fields based on planar nearfield acoustic holography,” *J. Acoust. Soc. Am.* **133**(6), 3885–3899.
- Robin, O., Berry, A., and Moreau, S. (2014). “Experimental vibroacoustic testing of plane panels using synthesized random pressure fields,” *J. Acoust. Soc. Am.* **135**(6), 3434–3445.
- Robin, O., Berry, A., and Moreau, S. (2015). “Experimental synthesis of spatially-correlated pressure fields for the vibroacoustic testing of panels,” in *International Conference on Flow Induced Noise and Vibration Issues and Aspects* (Springer, Berlin), pp. 151–185.
- Wilson, E. L., Der Kiureghian, A., and Bayo, E. (1981). “A replacement for the srss method in seismic analysis,” *Earthquake Engng. Struct. Dyn.* **9**(2), 187–192.